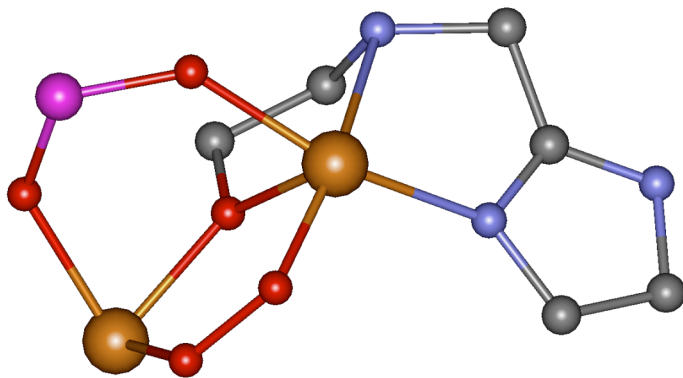
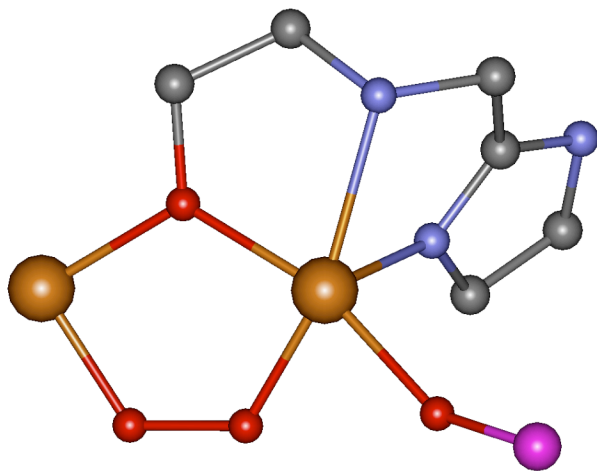


**Supporting Information**



**Figure S1.** FEFF models for **2•O<sub>2</sub>PPh<sub>2</sub>** and **2•O<sub>2</sub>AsMe<sub>2</sub>**, based on combination of crystal structures of **1•O<sub>2</sub>PPh<sub>2</sub>**, **1•O<sub>2</sub>AsMe<sub>2</sub>** and  $[\text{Fe}_2(\text{N-EtHPTB})(\text{O}_2)(\text{OPPh}_3)_2]^{3+}$  (Dong *et al.*)<sup>1</sup> using Accelrys DS Visualizer 1.7 and ChemBio 3D Ultra 11.0. Black = C, Blue = N, Red = O, Brown = Fe, Pink = P/As.



**Figure S2.** FEFF model for **3•O<sub>2</sub>PPh<sub>2</sub>**, based on crystal structures of  $[\text{Fe}_2(\text{N-EtHPTB})(\text{O}_2)(\text{OPPh}_3)_2]^{3+}$  (Dong *et al.*)<sup>1</sup> using Accelrys DS Visualizer 1.7 and ChemBio 3D Ultra 11.0. Black = C, Blue = N, Red = O, Brown = Fe, Pink = P.

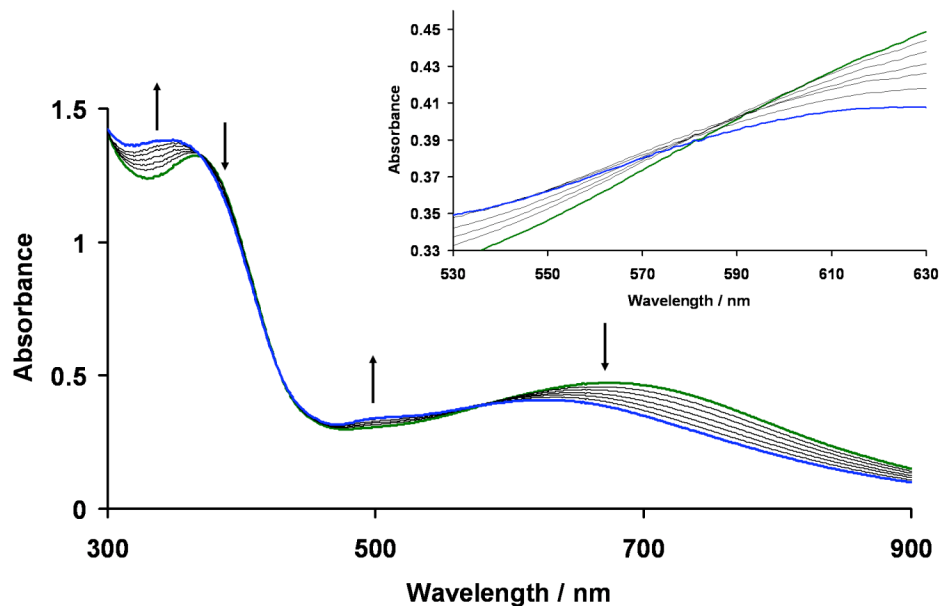


**Figure S3.** Partial conversion of a 0.5 mM solution of  $\mathbf{2}\bullet\text{O}_2\text{PPh}_2$  to  $\mathbf{3}\bullet\text{O}_2\text{PPh}_2$  in  $\text{CH}_2\text{Cl}_2$  in a 0.5 cm cuvette at -30 °C. The inset reveals the pseudo-isosbestic point at ~580 nm.

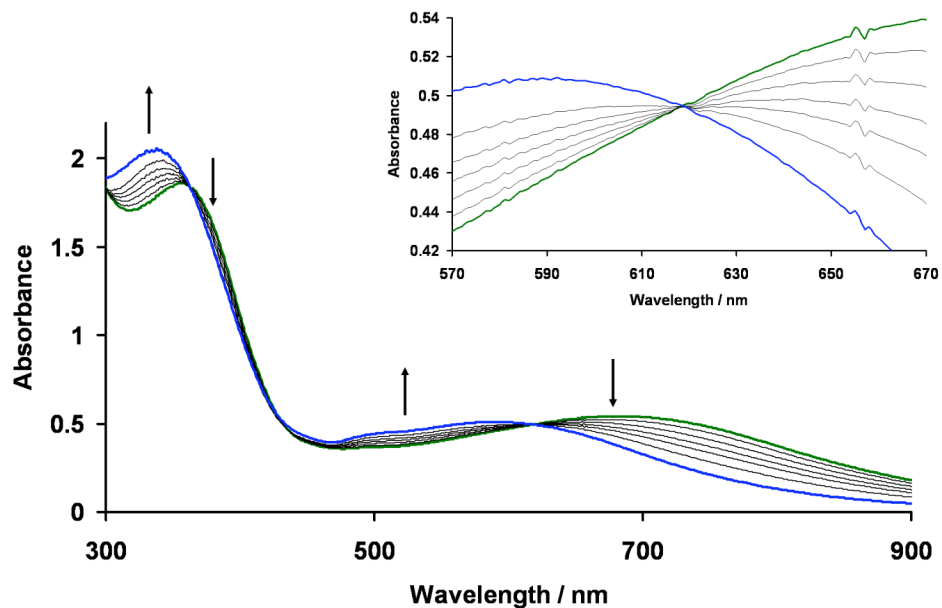


**Figure S4.** Conversion of a 0.5 mM solution of  $\mathbf{2}\bullet\text{O}_2\text{PPh}_2$  to  $\mathbf{3}\bullet\text{O}_2\text{PPh}_2$  in MeCN in a 0.5 cm cuvette at -30 °C. The inset reveals the isosbestic point at ~620 nm.

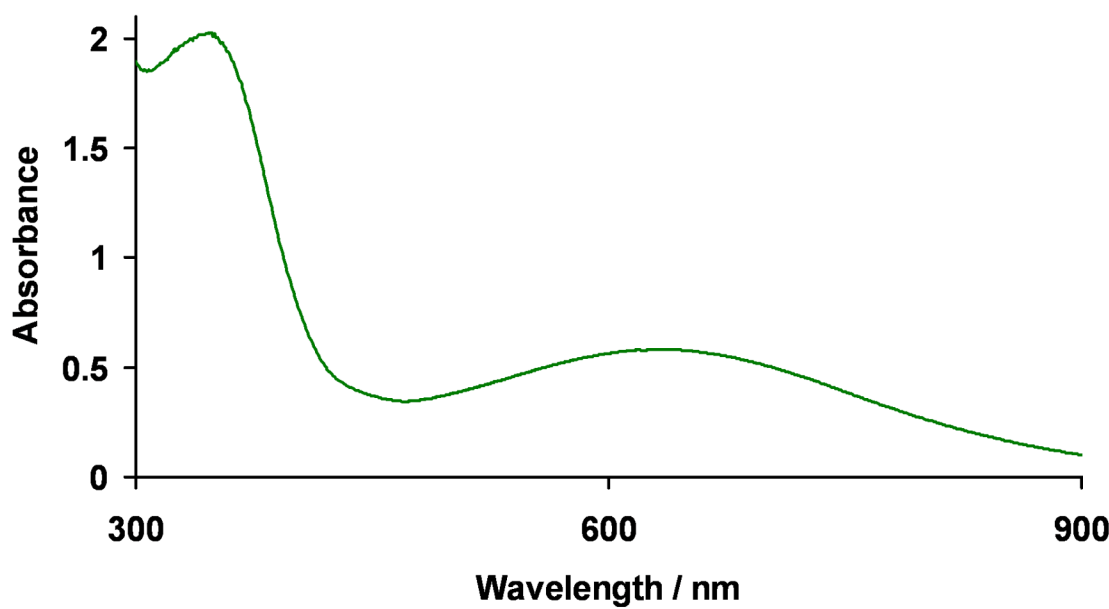


**Figure S5.** UV-Vis spectrum of a 0.5 mM solution of **2**•O<sub>2</sub>AsMe<sub>2</sub> in MeCN in a 0.5 cm cuvette at -40 °C.

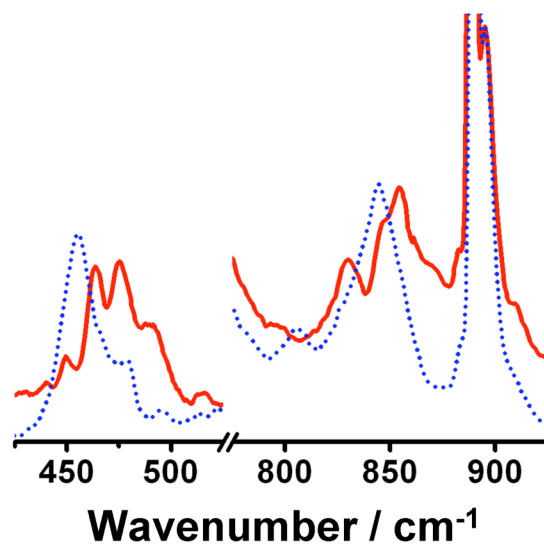


**Figure S6.** Resonance Raman spectra of frozen solutions of **3**•O<sub>2</sub>PPh<sub>2</sub> in CH<sub>2</sub>Cl<sub>2</sub>. Samples are contaminated with **2**•O<sub>2</sub>PPh<sub>2</sub>. Solid-red = <sup>16</sup>O<sub>2</sub>. Dotted-blue = <sup>18</sup>O<sub>2</sub>.

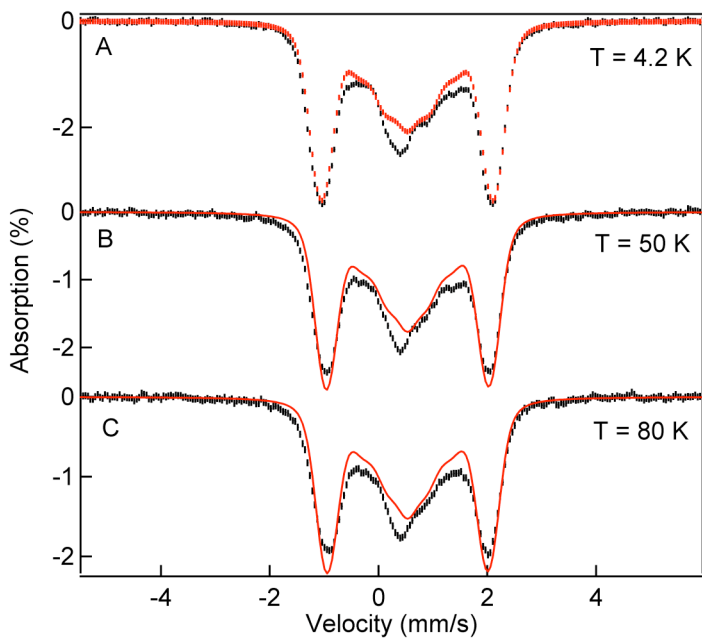


**Figure S7.** 8.0T Mössbauer spectra of  $\mathbf{3}\bullet\text{O}_2\text{PPh}_2$  in MeCN recorded at 4.2 K (A) and 50 K (B) and 80 K (C). The solid lines are theoretical curves using the parameters listed in Table 3. The solid line in (B) was obtained for  $J = 60 \text{ cm}^{-1}$ .

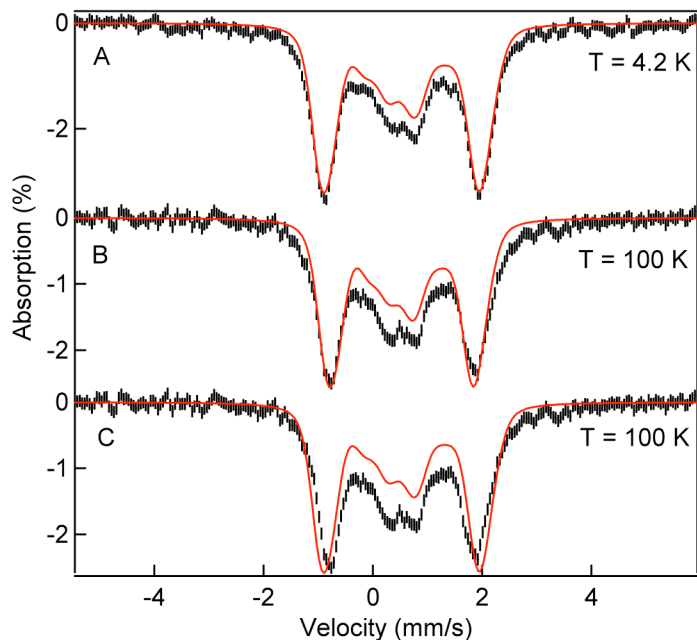


**Figure S8.** 8.0T Mössbauer spectra of  $\mathbf{3}\bullet\text{O}_2\text{PPh}_2$  in  $\text{CH}_2\text{Cl}_2$  recorded at 4.2 K (A) and 100 K (B). The solid lines are theoretical curves using the parameters listed in Table 3. The data in (C) are the same as in (B); the solid line in (C) is a simulation obtained by assuming that only the  $S = 0$  ground state is occupied at 100 K, i. e. using  $J = 1000 \text{ cm}^{-1}$ . The solid line in (B) was obtained for  $J = 60 \text{ cm}^{-1}$ .

**Table S1.** EXAFS fitting results for **2**•O<sub>2</sub>PPh<sub>2</sub>, **2**•O<sub>2</sub>AsMe<sub>2</sub>, and **3**•O<sub>2</sub>PPh<sub>2</sub>.<sup>a</sup>

Complex	Fit	Fe-O/N			Fe-O/N			Fe-O/N			Fe···C			Fe···X			F <sup>c</sup>	F <sup>d</sup>
		N	R	σ <sup>2</sup>	N	R	σ <sup>2</sup>	N	R	σ <sup>2</sup>	N	R	σ <sup>2</sup>	N	R	σ <sup>2</sup>		
<b>2</b> •O <sub>2</sub> PPh <sub>2</sub>	1	6	1.97	11.37													1.384	0.117
	2	5	2.00	8.64	1	2.30	1.13										1.225	0.104
	3	4	2.00	6.23	1	2.29	2.92				5	2.99	1.98				0.799	0.052
	4	4	2.00	6.32	1	2.29	2.00				5	2.98	3.84	1Fe	3.27	3.59	0.601	0.035
	5	4	1.99	6.14	1	2.29	3.31				5	2.94	10.66	1P	3.12	-0.30	0.488	0.023
	6	4	2.00	6.54	1	2.31	3.64				5	2.99	2.19	5C	2.21	2.26	0.662	0.042
	7	4	1.99	6.22	1	2.29	2.50				5	2.95	9.28	1Fe	3.24	9.60	0.430	0.022
	8	4	2.00	6.69	1	2.31	2.71	1	2.54	0.58	5	2.99	3.55	1Fe	3.28	3.18	0.392	0.018
	9	4	<b>2.00</b>	<b>6.57</b>	1	<b>2.30</b>	<b>1.50</b>	1	<b>2.51</b>	<b>3.00<sup>b</sup></b>	5	<b>2.96</b>	<b>7.95</b>	1Fe	<b>3.25</b>	<b>4.06</b>	<b>0.304</b>	<b>0.013</b>
<b>2</b> •O <sub>2</sub> AsMe <sub>2</sub>	1	6	1.94	14.63													1.517	0.149
	2	5	1.97	10.13	1	2.26	1.35										1.368	0.140
	3	5	1.99	10.86	1	2.25	0.12				3	2.97	-1.00				1.091	0.104
	4	5	1.97	10.82	1	2.25	2.19				3	2.93	3.86	1Fe	3.25	0.98	0.611	0.040
	5	5	1.97	10.95	1	2.26	2.85				3	2.90	7.46	1As	3.19	1.94	0.595	0.038
	6	5	1.97	10.66	1	2.25	1.03				3	2.95	1.63	6C	3.28	0.40	0.809	0.079
	7	3	<b>1.97</b>	<b>3.94</b>	2	<b>2.17</b>	<b>4.28</b>	1	<b>2.35</b>	<b>5.35</b>	3	<b>2.94</b>	<b>2.76</b>	1Fe	<b>3.27</b>	<b>1.24</b>	<b>0.381</b>	<b>0.018</b>
	8	3	<b>1.97</b>	<b>3.87</b>	2	<b>2.17</b>	<b>3.82</b>	1	<b>2.36</b>	<b>3.80</b>	3	<b>2.93</b>	<b>5.20</b>	1As	<b>3.21</b>	<b>2.24</b>	<b>0.369</b>	<b>0.019</b>
	9	3	1.97	3.85	2	2.17	3.89	1	2.35	4.24	3	2.92	3.34	1Fe	3.13	19.43	0.344	0.022
	10	3	1.97	3.84	2	2.17	3.90	1	2.36	4.71	3	2.94	2.22	1As	3.21	1.97		
<b>3</b> •O <sub>2</sub> PPh <sub>2</sub>	1	6	1.98	14.22													1.200	0.081
	2	5	2.00	7.84				1	1.84	1.30							1.143	0.083
	3	5	2.00	11.17	1	2.34	0.34										0.976	0.061
	4	4	2.03	5.68	1	2.34	1.01	1	1.87	1.16							0.914	0.061
	5	4	2.03	5.64	1	2.34	0.42	1	1.88	1.14	4	2.96	2.20				0.568	0.028
	6	4	<b>2.04</b>	<b>5.73</b>	1	<b>2.33</b>	<b>0.48</b>	1	<b>1.88</b>	<b>1.23</b>	4	<b>2.95</b>	<b>2.39</b>	1Fe	<b>3.47</b>	<b>4.59</b>	<b>0.366</b>	<b>0.012</b>
	7	4	2.04	5.74	1	2.33	0.52	1	1.88	1.28	4	2.95	2.30	1P	3.61	1.50	0.452	0.018
	8	4	2.03	5.73	1	2.33	0.67	1	1.88	1.24	4	2.95	2.63	5C	3.50	2.99	0.494	0.021
	9	4	2.04	5.58	1	2.33	0.80	1	1.88	1.12	4	2.95	2.43	1Fe	3.44	3.73	0.332	0.011
														0.5P	3.39	0.69		

<sup>a</sup> Resolution ~ 0.12 Å for **2**•O<sub>2</sub>PPh<sub>2</sub> and **3**•O<sub>2</sub>PPh<sub>2</sub> and ~ 0.14 Å for **2**•O<sub>2</sub>AsMe<sub>2</sub>; σ<sup>2</sup> = respective Debye-Waller factor in units of 10<sup>-3</sup> Å<sup>2</sup>.

<sup>b</sup> σ<sup>2</sup> value held fixed during optimization.

<sup>c</sup> F = goodness of fit calculated as  $F = \sqrt{\sum k^6 (\chi_{exp} - \chi_{cal})^2 / N}$ , where N = the number of data points.<sup>2</sup>

<sup>d</sup> F' = F<sup>2</sup>/ν, where ν = n<sub>idp</sub> - n<sub>var</sub>, n<sub>idp</sub> is the number of independent points in each data set and n<sub>var</sub> is the number of variables used in each optimization step. F' is used to indicate the improvement of fit upon the introduction of a shell.<sup>2</sup>

The  $\sigma^2$  values of the Fe···Fe path (1.24) and the Fe···As path (2.24) in **2**•O<sub>2</sub>AsMe<sub>2</sub> (Fits 7 and 8, respectively) are significantly smaller than the  $\sigma^2$  value of 4.06 found for the Fe···Fe paths in **2**•O<sub>2</sub>PPh<sub>2</sub> (Fit 9). Smaller  $\sigma^2$  leads to larger calculated amplitudes of Fe···Fe or Fe···As peaks in **2**•O<sub>2</sub>AsMe<sub>2</sub> as compared to the Fe···Fe path in **2**•O<sub>2</sub>PPh<sub>2</sub> (Figure S9). In fact, two Fe···Fe/As paths can also lead a good simulation of data in the k-range of 8 to 13 Å<sup>-1</sup> (Figure S10).

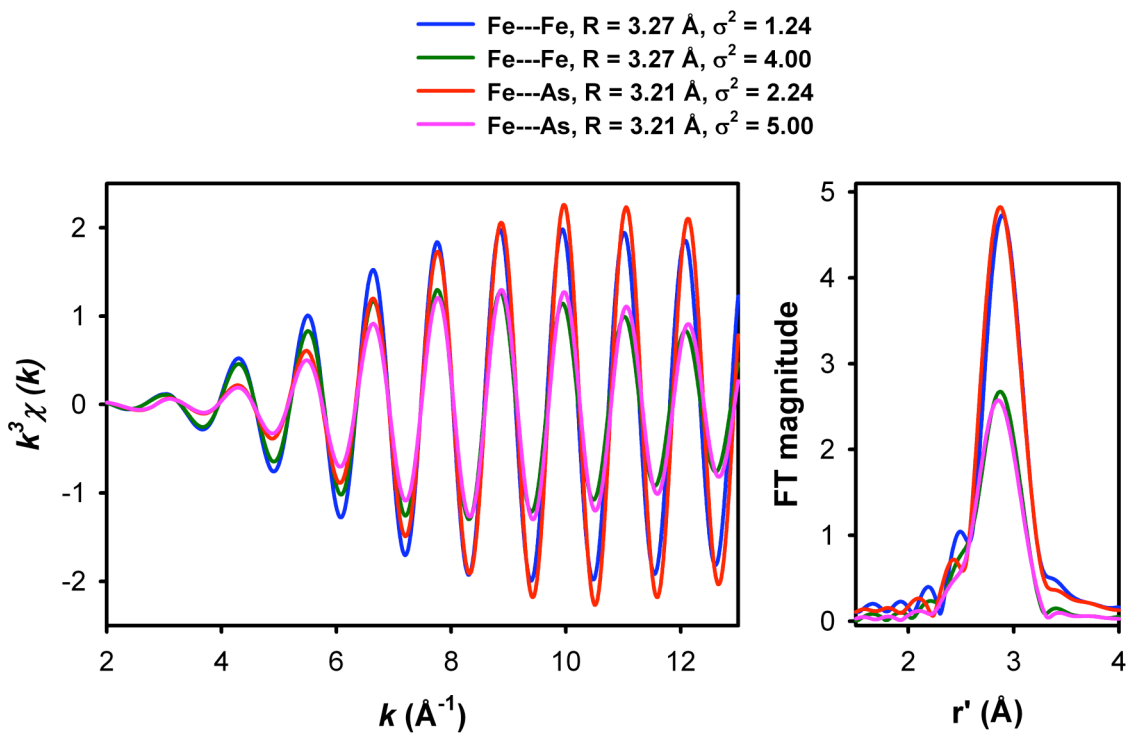


**Figure S9.** Theoretical EXAFS amplitudes and phases and FT amplitudes at different  $\sigma^2$  values using FEFF84\_87<sup>3,4</sup> and Artemis.<sup>5</sup>

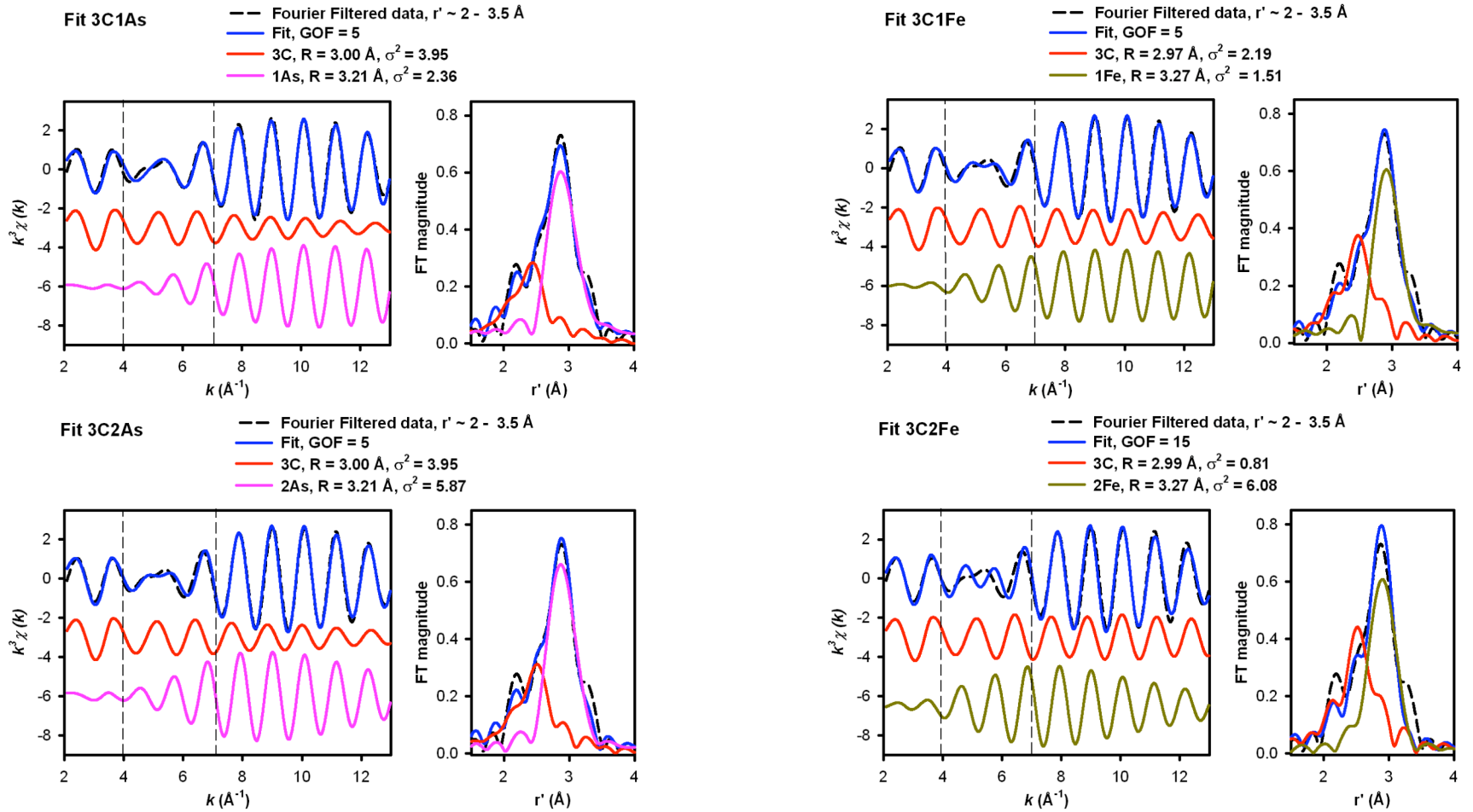


**Figure S10.** Fits to the outer shell with three Fe···C and one (3C1Fe, 3C1As) or two (3C2Fe, 3C2As) Fe···Fe/As paths. Fits 3C1Fe, 3C1As, and 3C2As are equally good. In fit 3C2Fe, the feature corresponding to the high Z scatterers is also well fitted. However, the destructive effect of two Fe···Fe paths on the 3 Fe···C paths in the range of 4 to  $7 \text{ \AA}^{-1}$  results in a lower quality of fit for 3C2Fe.

- (1) Dong, Y.; Yan, S.; Young, V. G., Jr.; Que, L., Jr. *Angew. Chem. Int. Ed. Engl.* **1996**, *35*, 618-620.
- (2) Riggs-Gelasco, P. J.; Stemmler, T. L.; Penner-Hahn, J. E. *Coord. Chem. Rev.* **1995**, *144*, 245-286.
- (3) Rehr, J. J.; Mustre de Leon, J.; Zabinsky, S. I.; Albers, R. C. *J. Am. Chem. Soc.* **1991**, *113*, 5135-5140.
- (4) Leon, J. M. d.; Rehr, J. J.; Zabinsky, S. I.; Albers, R. C. *Phys. Rev. B* **1991**, *44*, 4146-4156.
- (5) Ravel, B.; Newville, M. *J. Synchrotron Rad.* **2005**, *12*, 537-541.